EUSIPCO 2013 1569744163

A NOVEL TIME-FREQUENCY TECHNIQUE FOR MULTICOMPONENT SIGNAL DENOISING

T. Oberlin, S. Meignen

University of Grenoble and CNRS
Laboratoire Jean Kuntzmann
38 041 Grenoble cedex 09, France

S. McLaughlin

School of Engineering and Physical Sciences,
Heriot-Watt University, Edinburgh Scotland, UK

ABSTRACT

Multicomponent signals, i.e. superpositions of modulated waves, arise in many physical or biological systems. Exploiting the particular structure of these signals, denoising methods based on time-frequency distributions often outperform standard techniques such as those based on diagonal estimation or sparsity approaches. Recently, a simple denoising technique based on local integration in scale of the wavelet transform was proposed. In spite of its behaviour being better compared to classical techniques for medium noise levels, it does not perform so well in other cases. We propose here a method to improve denoising behaviour based on a more accurate mode reconstruction technique. The method is detailed for time-frequency representation given by short-time Fourier and continuous wavelet transforms, with the emphasis placed on their differences.

Index Terms— Time-frequency, ridge, synchrosqueezing, denoising, multicomponent signals

1. INTRODUCTION

Many signals from the physical world can be modeled as a sum of amplitude- and frequency-modulated (AM–FM) waves, called multicomponent signals, which have been the focus of much interest in the past few decades. As a result of their simplicity and efficiency, linear time-frequency (TF) transforms such as short-time Fourier transform (STFT) and continuous wavelet transform (CWT) have received particular attention. The STFT and CWT of multicomponent signals draw so-called *ridges* in the TF plane which, once detected, allow for the reconstruction of the different components by considering the transform on the ridges [1]. More recently, it was shown in [2, 3] that local frequency integration improved the robustness to noise of the reconstruction.

Yet, these methods do not perform very well when the frequency modulation is strong, i.e. when the modes locally behave like linear chirps. We propose here to adapt the size of the integration domain to frequency modulation and noise level.

Section 2 introduces the notation, and recalls the usual first-order approximation of the CWT and STFT of multicomponent signals. Then, section 3 extends these approximations to strong frequency modulations, while section 4 shows how to reconstruct the components in a noisy context. Finally numerical results are given in section 5, demonstrating the efficiency of the method on the one hand, and putting the emphasis on the differences between STFT and CWT on the other.

2. DEFINITIONS

2.1. Short-Time Fourier Transform

In the following, we denote by $L^1(\mathbb{R})$ and $L^2(\mathbb{R})$ the space of real integrable and square-integrable functions. Given a signal $s \in L^1(\mathbb{R})$, its Fourier transform is defined by:

$$\hat{s}(\eta) := \int_{\mathbb{R}} s(t)\, e^{-2i\pi\eta t}\, dt. \tag{1}$$

Taking a window $g \in \mathcal{S}(\mathbb{R})$, the (modified) Short-Time Fourier Transform (STFT) of a signal s is defined by

$$V_s(\eta, t) := \int_{\mathbb{R}} s(\tau) g(\tau - t) e^{-2i\pi\eta(\tau - t)}\, d\tau. \tag{2}$$

The STFT admits the following synthesis formula:

$$s(t) = \frac{1}{g(0)} \int_{\mathbb{R}} V_s(\eta, t)\, d\eta, \tag{3}$$

provided that $\eta \mapsto V_s(\eta, t)$ is integrable, which will always be the case in this paper.

2.2. Continuous Wavelet Transform

Taking an admissible wavelet $\psi \in L^2(\mathbb{R})$ (i.e. $C_\Psi := \int_0^\infty \frac{|\hat{\psi}(\xi)|^2}{\xi}\, d\xi < \infty$) and letting $\psi_{a,t}(\tau) := \frac{1}{a}\psi\left(\frac{\tau - t}{a}\right)$, we define the CWT of the signal s by:

$$\begin{aligned} W_s(a,t) &= \langle s, \psi_{a,t} \rangle \\ &= \frac{1}{a} \int_{\mathbb{R}} s(\tau)\, \overline{\psi\left(\frac{\tau - t}{a}\right)}\, d\tau, \end{aligned} \tag{4}$$

where $\bar{z}$ denotes the complex conjugate of z. We suppose that ψ is *analytic*, i.e. $\mathrm{Supp}(\hat{\psi}) \subset [0, \infty[$, so that the WT W_s of a real signal s is the half of the WT of its analytic signal $s_{an} = s + i\mathbf{H}(s)$, where $\mathbf{H}$ stands for the Hilbert transform (see [4] for details). We recall the Morlet formula (obtained by taking a Dirac for synthesis, see [4] for instance):

$$s_{an}(t) = \frac{1}{C'_\psi} \int_0^\infty W_s(a,t)\, \frac{da}{a}, \tag{5}$$

where $C'_\psi = \int_0^\infty \overline{\hat{\psi}(\xi)} \frac{d\xi}{\xi}$. The real signal is easily obtained by $s = \frac{1}{2}\mathcal{R}e(s_{an})$.

2.3. Multicomponent signals and ridges

A general modulated wave writes $h(t) = a(t)e^{2i\pi\phi(t)}$, with $a(t) > 0$ and $\phi'(t) > 0$. When a and ϕ' are slow-varying functions, both the CWT and STFT of such signals have been studied for decades, and can be well approximated in the vicinity of time t by considering the pure wave

$$\tilde{h}_1(t+\tau) = a(t)e^{2i\pi[\phi(t)+\phi'(t)\tau]}. \tag{6}$$

We then get

$$\begin{array}{rcl} V_h(\eta,t) & \approx & h(t)\,\hat{g}(\eta - \phi'(t)) \\ W_h(a,t) & \approx & h(t)\,\hat{\psi}(a\phi'(t)), \end{array} \tag{7}$$

The frequency center of ψ being assumed to be one without any loss of generality. Dealing with multicomponent signals, i.e. superpositions of modes, is no more complicated as soon as the different components are *separated* in frequency, which means their TF distribution do not overlap. Let $s(t) = \sum_{k=1}^K a_k(t)e^{2i\pi\phi_k(t)}$ be a multicomponent signal, we recall the separation condition for both STFT and CWT:

Proposition 2.1. *The signal s is separated for STFT if*

$$|\phi'_k(t) - \phi'_l(t)| > \mathrm{Supp}\,\hat{g},\ k \neq l, \tag{8}$$

and for CWT if

$$\frac{|\phi'_k(t) - \phi'_l(t)|}{|\phi'_k(t) + \phi'_l(t)|} > \frac{1}{2}\,\mathrm{Supp}\,\hat{\psi},\ k \neq l, \tag{9}$$

where $\mathrm{Supp}\,\hat{g}$ (resp. $\hat{\psi}$) denotes the size of the frequency bandwidth of g (resp. ψ). The difference arises here because of the logarithmic frequency description used by CWT. Also, studying separated multicomponent signals amounts to studying single components, which we will do in the sequel.

2.4. Gaussian window and wavelet

Due to its optimal TF resolution, the Gaussian function is often used as window g. Let us define the Gaussian window and its corresponding complex Gaussian (also called Morlet) wavelet:

$$g(t) = \sigma^{-1/2} e^{-\pi \frac{t^2}{\sigma^2}}, \tag{10}$$

$$\psi(t) = \sigma^{-1/2} e^{-\pi \frac{t^2}{\sigma^2}} e^{2i\pi t}. \tag{11}$$

The parameter σ enables the choice of the size of the window/wavelet in accordance with (8) and (9). The next section shows how to use these particular functions to extend approximations (7) to the case of strong frequency modulations.

3. RECONSTRUCTING STRONG FREQUENCY-MODULATED SIGNALS

Let us now assume that $\phi''(t)$ is no longer negligible, then first order approximations (7) no longer hold, and more involved techniques are needed. For that purpose, an asymptotic method in time domain, the stationary phase approximation, has been used successfully in [1]; a different technique introduced in [5] is to expand the phase up to the second order. The next section derives the corresponding approximation of the STFT and CWT magnitude, on which our denoising technique is based.

3.1. Exact formulae for a Gaussian window/wavelet

We now aim to extend formulae (7) when the frequency modulation is not negligible. The simplest way to proceed is to approximate the mode h in the vicinity of t by its second-order Taylor expansion:

$$\tilde{h}_2(t+\tau) = a(t)e^{2i\pi[\phi(t)+\phi'(t)\tau+\frac{1}{2}\phi''(t)\tau^2]}. \tag{12}$$

To study the STFT of such chirps, we need to compute the Fourier transform of a Gaussian modulated linear chirp.

Proposition 3.1. *Consider the function $u(t) = e^{-\pi z t^2}$, where $z = re^{i\theta}$ with $\cos\theta > 0$, so that the function is integrable. Then its Fourier transform is*

$$\hat{u}(\xi) = r^{-\frac{1}{2}} e^{-i\frac{\theta}{2}} e^{-\frac{\pi}{re^{i\theta}}\xi^2}. \tag{13}$$

Proof. One can proceed as in the case when z is real: it suffices to differentiate u and consider the Fourier transform of the obtained differential equation (see Appendix A of [6] for instance). □

Theorem 3.1. *For a Gaussian window or its associated Morlet wavelet, the magnitude of the STFT and CWT transform of $\tilde{h}_2$ admits the following closed-form expressions:*

$$|V_{\tilde{h}_2}(\eta,t)| = |h(t)|\sigma^{\frac{1}{2}}(1+\sigma^4\phi''(t)^2)^{-\frac{1}{4}} e^{-\frac{\pi\sigma^2(\eta-\phi'(t))^2}{1+\sigma^4\phi''(t)^2}}$$

$$|W_{\tilde{h}_2}(a,t)| = |h(t)|\sigma^{\frac{1}{2}}(1+\sigma^4 a^4\phi''(t)^2)^{-\frac{1}{4}} e^{-\frac{\pi\sigma^2(1-a\phi'(t))^2}{1+\sigma^4 a^4\phi''(t)^2}}.$$

Proof. For a fixed time t, equation (12) and Proposition 3.1 give

$$V_{\tilde{h}_2}(\eta,t) \quad = \quad h(t)\sigma^{-\frac{1}{2}}r^{-\frac{1}{2}}e^{-i\frac{\theta}{2}}e^{-\frac{\pi}{r}e^{-i\theta}(\eta-\phi'(t))^2}, \quad (14)$$

with $r=(\frac{1}{\sigma^4}+\phi''(t)^2)^{\frac{1}{2}}$ and $\theta=\arctan(-\phi''(t)\sigma^2)$. Using the identity $\cos\arctan x = \frac{1}{\sqrt{1+x^2}}$, one finally obtains $V_{\tilde{h}_2}$, and $W_{\tilde{h}_2}$ in the same manner. □

This shows that the magnitude of the STFT of a linear chirp is also a Gaussian function centered in $\eta=\phi'(t)$. The difference with equations (7) lies in the magnitude and the width of this Gaussian. The formula for the CWT is very similar, except that σ is replaced by $a\sigma$.

3.2. Stationary phase approximation

We have explicit formulae for the STFT and the CWT of a linear chirp, when both g and ψ are Gaussian. However, in a more general context such formulae are no longer available, but the transforms can still be well approximated by the stationary phase approximation [7]. Let us suppose that $\phi'(t)$ is strictly monotonic, then for any (η,t) there exists at most one time t_c such that $\phi'_k(t_c)=\eta$. If t_c exists, then the stationary phase approximation gives

$$|V_h(\eta,t)| \approx |h(t_c)|\frac{g(t_c-t)}{\sqrt{|\phi''(t_c)|}}. \quad (15)$$

We can conduct the same reasoning with the CWT, where η is replaced by $1/a$, which gives

$$|W_h(a,t)| \approx |h(t_c)|\frac{\left|\psi\left(\frac{t_c-t}{a}\right)\right|}{a\sqrt{|\phi''(t_c)|}}. \quad (16)$$

The method presented here can be adapted to any general window, using these formulae.

4. DENOISING MULTICOMPONENT SIGNALS

The previous section gave details about how the information is localised around the ridges. We aim here at using this information for denoising ; so we consider a multicomponent signal corrupted by a white Gaussian noise. To denoise the signal we propose the following method, also used in [3]:

- Estimate the ridge at time t, $\phi'(t)$.
- Compute the integration domains $\mathcal{I}(t)$, so that for $\eta\in\mathcal{I}(t)$, $|V_h(\eta,t)|$ is higher than the noise level.
- Integrate the STFT or CWT of the noisy signal on the domain, to get an estimate of $h(t)$.
- Iterate the process for all times t and all components.

This process is illustrated in Figure 1, where the STFT and CWT of an AM–FM mode are displayed along with a slice of both transforms for a fixed time, showing the integration domain. The following sections will explain how to choose the frequency integration domains $\mathcal{I}(t)$, considering either the first- or second-order approximation.

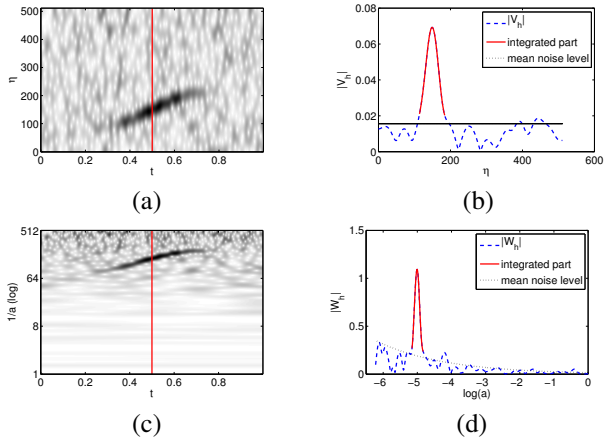

Fig. 1. Illustration of STFT- or CWT-based denoising. (a) STFT of a noisy AM–FM wave. (b) a slice of the STFT at time $t=\frac{1}{2}$, along with the mean noise level and the integrated part. (c) and (d): idem for CWT, scales being displayed on a logarithmic scale.

4.1. Noise distribution in the transformed domain

Let us start by quantifying the noise distribution on STFT and CWT. We consider a noisy realisation $s(t)=h(t)+n(t)$, where n is a Gaussian process with 0 mean and variance σ_n^2. For a fixed frequency η or scale a, a simple calculation leads to

$$\begin{array}{rcl}\mathrm{Var}(|V_n(\eta,t)|) & = & \sigma_n^2 \\ \mathrm{Var}(|W_n(a,t)|) & = & \frac{1}{a}\sigma_n^2.\end{array} \quad (17)$$

4.2. Integration domain, first order

According to equation (7), $\eta\mapsto|V_h(\eta,t)|$ almost reaches a maximum at $\phi'(t)$, and is symmetric with respect to $\phi'(t)$. Thus, we aim at computing $\Delta_{1,V}$ such that $|V_h(\phi'(t)\pm\Delta_{1,V},t)| = \sigma_n$. Using equation (17) and remarking that $\sqrt{\sigma}|h(t)| = |V_h(\phi'(t),t)| = V_{max}(t)$, we get

$$\Delta_{1,V} = \frac{1}{\sigma\sqrt{\pi}}\sqrt{-\log\frac{\sigma_n}{V_{max}(t)}}. \quad (18)$$

To compute the analogue for the CWT leads to integrate on $[\frac{1-\Delta_{1,W}}{\phi'(t)},\frac{1-\Delta_{1,W}}{\phi'(t)}]$, with

$$\Delta_{1,W} = \frac{1}{\sigma\sqrt{\pi}}\sqrt{-\log\left(\frac{\sigma_n}{W_{max}(t)\sqrt{a}}\right)}, \quad (19)$$

where $a=\frac{1\pm\Delta_{1,W}}{\phi'(t)}$ is the corresponding scale. An easy way to remove a from the right-hand side is to approximate a by $\phi'(t)$.

4.3. Second order model

A similar computation for the second-order model gives

$$\begin{aligned}\Delta_{2,V} &= \frac{\sqrt{1+\sigma^4\phi''(t)^2}}{\sigma\sqrt{\pi}}\sqrt{-\log\frac{\sigma_n}{V_{max}(t)}},\\ \Delta_{2,W} &= \frac{\sqrt{1+a^4\sigma^4\phi''(t)^2}}{\sigma\sqrt{\pi}}\sqrt{-\log\left(\frac{\sigma_n}{W_{max}(t)\sqrt{a}}\right)},\end{aligned} \tag{20}$$

where we can still use the approximation $a \approx \phi'(t)$.

5. NUMERICAL RESULTS

This section shows the efficiency of the denoising method on synthetic signals. Methods will be denoted by STFT1, STFT2, CWT1 or CWT2, depending on the transform and the approximation order. We will compare them with a general TF denoising technique: Block-Thresholding [8], denoted by BT hereafter. Ridges are estimated using a simple heuristic search like in [5], whereas $\phi_k''(t)$ is estimated by ridge differentiation after a regularizing spline-fitting step. The code implementing the method can be downloaded from `http://www-ljk.imag.fr/membres/Thomas.Oberlin/Eusipco13.tar.gz`, together with Matlab scripts that plot all the figures of this paper.

5.1. A first example

Let us first assess the efficiency of first-order methods. Figure 2 (a) and (b) show the STFT and CWT of a low-modulated 3-component signal. Denoising results for this signal are depicted on Figure 2 (c); they show that STFT1 and CWT1 clearly outperform BT for any input SNR. Note however that the method does not work for very high noise levels ($SNR < -5dB$), since the ridges are no longer correctly estimated.

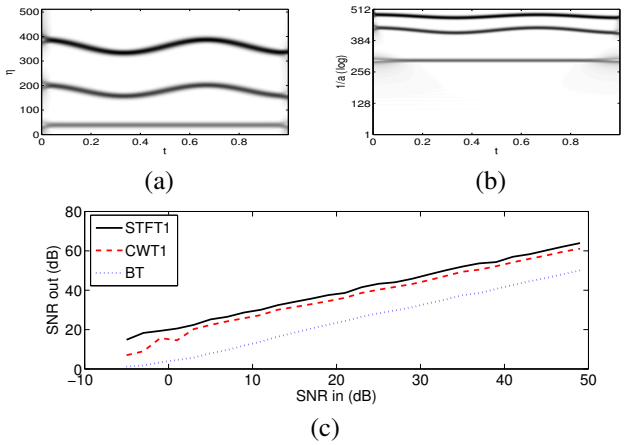

Fig. 2. Denoising performances on a synthetic 3-components signal. (a) STFT with window $\sigma = 0.05$. (b) CWT with $\sigma = 7$. (c) comparison between 3 methods.

5.2. STFT vs CWT, and window's size

Let us here stress the differences between STFT and CWT. First, note that the denoising performance depends on the ability of the transform to *sparsely* represent the signal. If the signal is made of monochromatic waves, taking a large window will ensure a quasi-perfect TF representation (i.e., made of three thin lines). But if the components are frequency modulated, a very large window will cause strong time diffusion, which hampers the quality of the representation. Thus, one has to choose σ so as to achieve a trade-off between time and frequency localization.

The main difference between STFT and CWT lies in how they handle frequency modulation: STFT performs well provided ϕ'' is low, whereas CWT needs ϕ''/ϕ' to be low (see the discussion in [4] section 4.5 for more details). The other difference concerns mode separation condition (equations (8) and (9)), which must be linear for STFT and logarithmic for CWT. This is illustrated here through the study of two different 3-component signals: one is composed of polynomial chirps and is well adapted to STFT, whereas the other contains exponential chirps that can be well processed by CWT. The STFT and CWT of both signals are displayed in Figure 3, together with their respective denoising performances using the second-order approximation. Figure 3 (c) shows that methods based on STFT representation are well adapted to polynomial chirps, whereas a poor separation in the time-scale plane hampers CWT2. However, according to Figures 3 (d) and (f), STFT-based methods do not manage to denoise the signal properly because of heavy time diffusion effects. Note parameters σ are chosen carefully for each method to get the best possible results, i. e. they must ensure that (8) and (9) are satisfied. .

5.3. Contribution of the second-order model

This section illustrates how to take into account second-order terms enables better signal denoising in case of strong frequency modulation. For this purpose, the two signals of Figure 3 are denoised using either the first or second order methods, and the results are displayed in Figure 4. This shows that the second-order approximation offers little improvement when the noise level is high, but is of great interest for low noise.

6. CONCLUSION

This paper analysed the magnitude of the STFT and CWT of strongly modulated multicomponent signals for signal denoising. A component reconstruction method by local integration was proposed which took into account local frequency modulation and noise level. Numerical experiments demonstrated the effectiveness of the approach for the denoising of multicomponent signals with polynomial or exponential phase, respectively from their STFT or CWT.

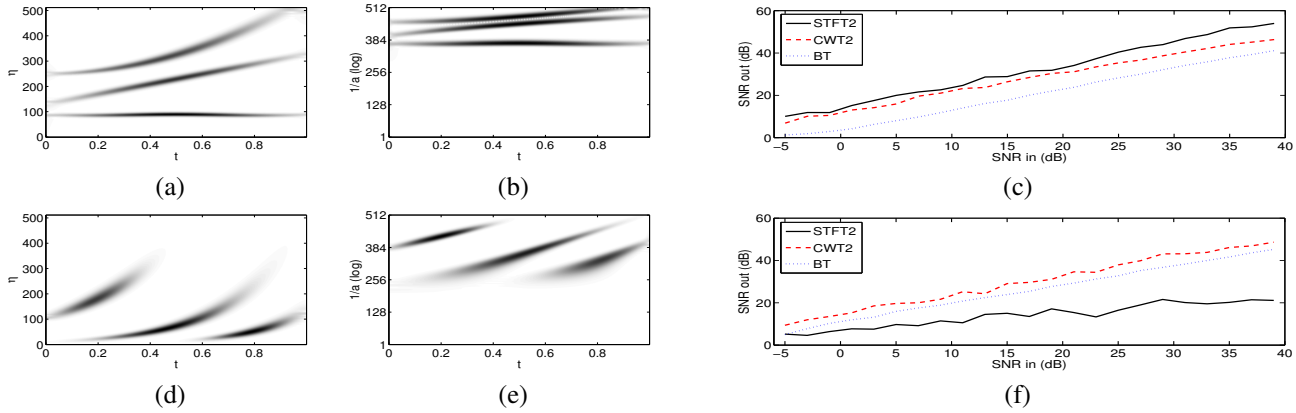

Fig. 3. Analysis of signals with strong frequency modulations. (a): STFT of a superposition of polynomial chirps; (b): CWT of the same signal; (c): corresponding denoising results for STFT2 and CWT2. (d), (e) and (f): STFT, CWT and corresponding denoising performance for a superposition of exponential chirps. The parameters are $\sigma = 0.08$ for STFT and $\sigma = 5$ for CWT.

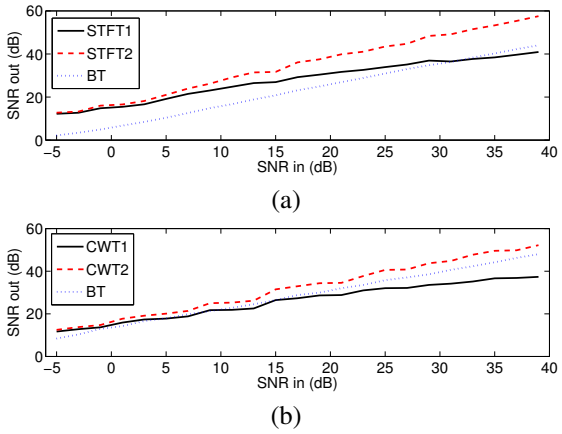

Fig. 4. Importance of second-order terms for strong frequency modulation. (a): denoising performance for STFT1 and STFT2 applied to the signal of Figure 3 (a) and (b), with $\sigma = 0.08$. (b): denoising performance for CWT1 and CWT2 applied to the signal of Figure 3 (d) and (e), with $\sigma = 5$.

Future works should include a broader comparison with other denoising methods, based for instance on the Wigner-Ville transform [9], wavelet packet dictionaries [10] or the Empirical Mode Decomposition [11].

References

[1] N. Delprat, B. Escudié, P. Guillemain, R. Kronland-Martinet, P. Tchamitchian, and B. Torrésani, "Asymptotic wavelet and Gabor analysis: Extraction of instantaneous frequencies," *Information Theory, IEEE Transactions on*, vol. 38, no. 2, pp. 644–664, 1992.

[2] S. Meignen, T. Oberlin, and S. McLaughlin, "A new algorithm for multicomponent signals analysis based on synchrosqueezing: With an application to signal sampling and denoising," *Signal Processing, IEEE Transactions on*, vol. 60, no. 11, pp. 5787 –5798, nov. 2012.

[3] S. Meignen, T. Oberlin, and S. McLaughlin, "Multicomponent signal denoising with synchrosqueezing," in *Statistical Signal Processing Workshop (SSP), 2012 IEEE*, aug. 2012, pp. 660 –663.

[4] S. Mallat, *A wavelet tour of signal processing*, Academic Press, 1999.

[5] T. Oberlin, S. Meignen, and S. McLaughlin, "Analysis of strongly modulated multicomponent signals with the short-time Fourier transform," in *Proceedings of ICASSP*, 2013.

[6] D.W. Kammler, *A first course in Fourier analysis*, Cambridge University Press, 2008.

[7] N. Bleistein, A. Richard, et al., *Asymptotic expansions of integrals*, Dover Publications, 2010.

[8] G. Yu, S. Mallat, and E. Bacry, "Audio denoising by time-frequency block thresholding," *Signal Processing, IEEE Transactions on*, vol. 56, no. 5, pp. 1830–1839, 2008.

[9] L.J. Stankovic and V. Katkovnik, "The Wigner distribution of noisy signals with adaptive time-frequency varying window," *Signal Processing, IEEE Transactions on*, vol. 47, no. 4, pp. 1099–1108, 1999.

[10] H. Krim, D. Tucker, S. Mallat, and D. Donoho, "On denoising and best signal representation," *Information Theory, IEEE Transactions on*, vol. 45, no. 7, pp. 2225–2238, 1999.

[11] Y. Kopsinis and S. McLaughlin, "Development of EMD-based denoising methods inspired by wavelet thresholding," *Signal Processing, IEEE Transactions on*, vol. 57, no. 4, pp. 1351–1362, 2009.